

NPS ARCHIVE
1964
TOPPING, R.

AN INVESTIGATION OF THE RADIAL
DISTRIBUTION OF LIGHT FROM
AN ARGON DISCHARGE

ROBERT L. TOPPING

DUDLEY KNOX LIBRARY
NAVAL POSTGRADUATE SCHOOL
MONTEREY, CA 93943-5101

Library
Naval Postgraduate School
Monterey, California

34

AN INVESTIGATION OF THE
RADIAL DISTRIBUTION OF LIGHT
FROM AN ARGON DISCHARGE

* * * * *

Robert L. Topping

AN INVESTIGATION OF THE
RADIAL DISTRIBUTION OF LIGHT
FROM AN ARGON DISCHARGE

by

Robert L. Topping
Lieutenant, United States Navy

Submitted in partial fulfillment of
the requirements for the degree of

MASTER OF SCIENCE

IN

PHYSICS

United States Naval Postgraduate School

Monterey, California

1964

S. Archive

64

opping, R.

~~IN~~

Library
U. S. Naval Postgraduate School
Monterey, Calif. 94034

AN INVESTIGATION OF THE
RADIAL DISTRIBUTION OF LIGHT
FROM AN ARGON DISCHARGE

by

Robert L. Topping

This work is accepted as fulfilling
the thesis requirements for the degree of

MASTER OF SCIENCE

IN

PHYSICS

from the

United States Naval Postgraduate School

ABSTRACT

The light intensity distributions in the positive column of a cylindrical argon discharge were observed in order to determine the radial distributions of the emitters of this detected light. A collimated beam of light originating in the discharge was observed using the 1P28 as the detector. The transformation of the data from the observed intensity profiles to radial distributions was accomplished by the use of a method proposed by W. L. Barr.

It was observed that :

- a. the normalized radial distribution of emitters shows a regular variation with greater constriction at lower currents (constant pressure) or higher pressure (constant current).
- b. as currents increased and/or pressure decreased, the distribution of emitters approached the zero order Bessel function distribution.
- c. no significant variation of radial emitter distribution could be associated with the presence or absence of striations.

TABLE OF CONTENTS

Section	Title	Page
I.	Introduction	1
1.	Subdivisions of Gaseous Discharges	1
1.1	Dark Discharges	2
1.2	Glow Discharges	2
1.3	Arc Discharges	3
2.	Positive Column	4
II.	Radial Distributions	6
1.	Theories of Radial Distributions within a Column	6
2.	Previous Calculations of Radial Distributions of Emitters	7
3.	Procedure	9
4.	Analysis of Data	11
5.	Results	13
6.	Recommendations for Further Work	14
7.	Acknowledgements	15
	Bibliography	16
	Appendix I	17
	Appendix II	20
	Appendix III	27

LIST OF ILLUSTRATIONS

Figure	Page
1. Classification of Discharges	1
2. Radial Distribution of Electron (T_e) and Gas (T_g) Temperature at Various Pressures	6
3. Illustration of the Geometrical Relationships between Variables	7
4. Parameters of the Analyzed Discharges	10
5. Cone of Light Falling on the Photomultiplier Surface	13
6. Schematic Diagram of Power Supply	31
7. Schematic Diagram of Vacuum System	31
8. Overall View of the Equipment	33
9. Close View of Scanning Device	33
10. View of Working Platform	34
11. View of Diffusion Pump and Forepump	34
12. Close View of Tubes 1 and 2	35

CHAPTER I

INTRODUCTION

1. Subdivisions of Gaseous Discharges

The electric gas discharge is a phenomenon which is observed when a gas or vapor becomes able to conduct electrical currents; that is, when the gas is ionized. Under these conditions free electric charges are present and can move through the gas, usually under the influence of an electrical field.⁽¹⁾

Gas discharges are classified into several categories determined by their current and voltage. The graph below shows the divisions of these discharges.⁽²⁾ It is convenient to regard the dark discharge, the glow discharge, and the arc discharge as three fundamental types of continuous electric discharges.

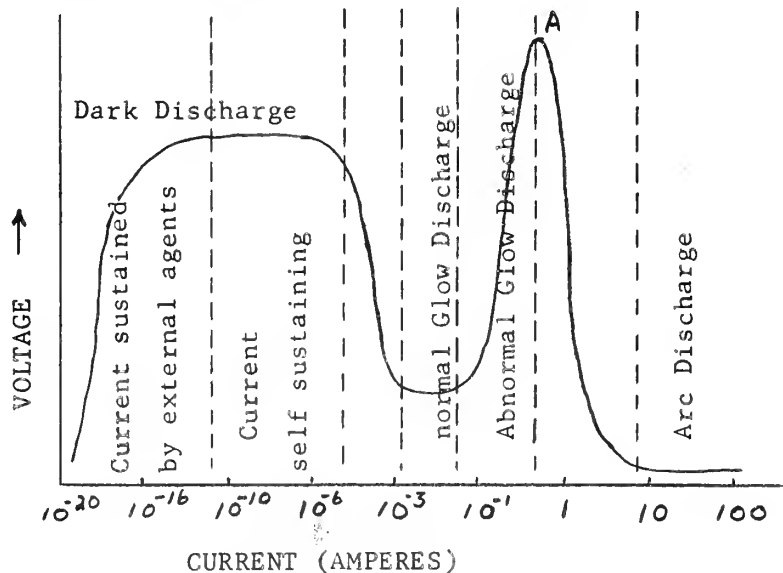


Figure 1

The discharge systems in this work were in the transition region between the glow discharge and the arc discharge region (0.3 - 1.3 amperes).

1.1 Dark Discharges

It will be sufficient here to note that if a dark discharge has a sufficiently large reduced field ($\frac{E}{p}$) to cause ionization and too few atoms with high electron affinities to dampen critically any initiated discharge, it will be self sustaining. If it is not a self sustaining discharge, the discharge compensates for its inability to multiply effectively the number of electrons and ions by relying on the charges created by the external agents.

1.2 Glow Discharges

Electrons required for the continuance of the glow discharges are produced by the bombardment of the cathode primarily by positive ions, but also by metastable atoms, fast atoms (charge transfer), and electromagnetic radiation. To discuss the characteristics of a glow discharge, higher current densities than the dark current discharge must be considered, and the effects of space charge are all important. Space charge largely determines the electric field.

The major characteristics of each space in the glow discharge are described below primarily in terms of the distribution of emitted light.

A secondary electron usually starts at the cathode with very little initial speed. It will not be able to excite gas molecules until its energy is at least equal to the excitation energy. This region where the electron is gaining the energy required for excitation is called the Aston dark space. Electrons reach an energy corresponding to the maximum of the excitation probabilities in the cathode glow region. Beyond the cathode glow they have speeds

far beyond the maximum of the excitation probabilities and thus very little light is emitted from the cathode dark space (Crookes dark space). Many collisions take place in the cathode dark space creating many slow electrons. These slow electrons have gained sufficient energy to excite atoms upon reaching the negative glow region. Afterwards their energy becomes small and recombinations with positive ions can take place. These electrons are therefore slow when leaving the negative glow space and are slowed some more by the small negative space charge. Going toward the anode the field rises slowly and the probability of recombination decreases, and the Faraday dark space develops. Since the field is found to increase in the direction of the positive column, spectral lines will again start appearing when sufficient energy has been gained. This energy is available upon entering the positive column. The positive column has a constant field and space charge and therefore gives a uniform appearance. In the last few mean free paths, the electrons may gain a high enough average energy to excite more freely, producing the anode glow. The excess of electrons in front of the anode tends to slow the electrons down thus creating the anode dark space.

1.3 Arc Discharges

The glow-to-arc transition can be accomplished by increasing the current of the glow until there is a sufficient number of ions hitting the cathode to heat it to the point that thermionic emission from the cathode becomes comparable to electron emission by bombardment. This corresponds to point A of Figure 1. The type of discharge studied in this work employed the thermionic effect in which

the cathode was heated by an external source and the arc was not self sustaining, except by increasing the tube voltage. The main electrical property of an arc is that for a given discharge tube, the arc voltage decreases as the current rises.⁽¹⁾ The axially symmetric arc discharge is filled with a tenuous plasma. This stretches from near the cathode to the anode and is called the positive column. In this work the distributions of emitters were investigated in the positive column only. The distributions should be the same for an arc or glow discharge except perhaps for the ends of the column where the gas may contain a certain amount of vapor from the cathode and anode material in the arc discharge.

2. Positive Column

Since the discharges were investigated in the positive column region, the following properties of the positive column deserve consideration.

2.1 Optically Thin Plasma

Results of this work are based on the assumption that the positive column is optically thin. The following calculations indicate this to be a very good assumption.

The attenuation distance (d) of a wave in a plasma when ν_m is not equal to zero is ⁽⁴⁾ $d = 2c\omega(\omega^2 - \omega_p^2)^{1/2} / \nu_m \omega_p^2$. The plasma angular frequency (ω_p) is given by ⁽³⁾ $\omega_p = \left(\frac{4\pi n}{m}\right)^{1/2} e$. $\omega_p / 2\pi$ is at most 10^{10} cycles per second in discharges studied in this work.⁽¹⁰⁾ The attenuation distance for 3400 Angstrom light (the 1P28 is most sensitive at about 3400 Angstroms) is then $d = 7 \times 10^{-3}$ meters. Therefore absorption due to plasma frequency is negligible.

No experiments were conducted in this work to determine the

amount of trapping of resonance radiation. However, it should be noted that there are but two metastable states of argon and only one transition (the 3949 line)⁽⁶⁾ to a metastable state is possible in the range of maximum sensitivity of the photomultiplier. Therefore, we expect no significant trapping of resonance radiation within the region of sensitivity of the 1P28 photomultiplier.

CHAPTER II

RADIAL DISTRIBUTIONS

1. Theories of Radial Distributions Within A Column

von Engel⁽¹⁾ has calculated that the radial distribution of ions or electrons at a distance r from the axis of a cylindrical discharge is: $N_r = N_0 J_0(2.405 r/R)$ Eq. II.1.1

This relation is based on the assumptions:

- a. that electron mean free path is much less than the tube radius R , i.e., that diffusion laws apply.
- b. that the loss of electrons and ions by diffusion is so nearly the same (ambipolar diffusion) that $N^+ = N^- = N$
- c. that electrons and ions do not recombine in the gas, but neutralize their charges on the wall. Hence this implies their concentration is large at the axis and practically zero at the wall.

The radial distribution of temperature is another consideration affecting this study. Figure 2 below shows the expected radial distributions of temperature for three various pressure ranges.⁽¹⁾

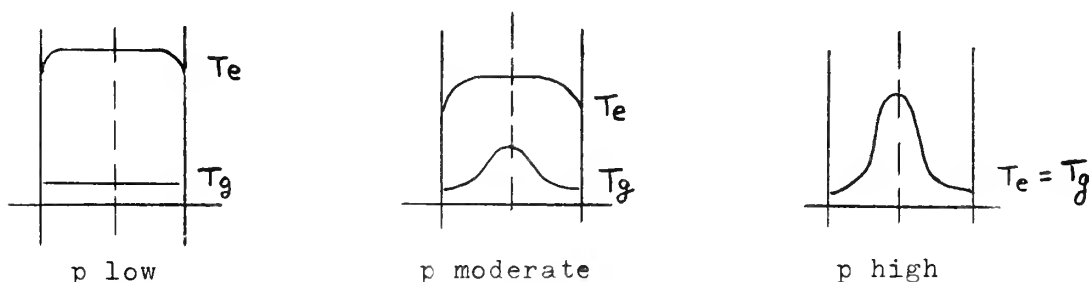


Figure 2

Radial distribution of electron(T_e) and gas (T_g) temperature
at various pressures.

Since no measurements of gas and electron temperature were made, it is not possible to state what distribution of temperature was present, other than to note that these runs were at low or moderate pressures.

2. Previous Calculations of Radial Distributions of Emitters

Since the photomultiplier used to observe the positive column uses radiant energy coming from a range of depths, a method of converting this total intensity to a radial distribution was required. Barr⁽⁷⁾ and Bockasten⁽⁵⁾ have reported methods to convert observed radiation intensity profiles from an optically thin cylindrical source into a function for the radial distribution of emitters.

Consider a detector equipped with a collimating system of slits so that it accepts only that energy which originates within a narrow slice through the discharge and is directed into the entrance aperture of the collimator. (See Figure 3)

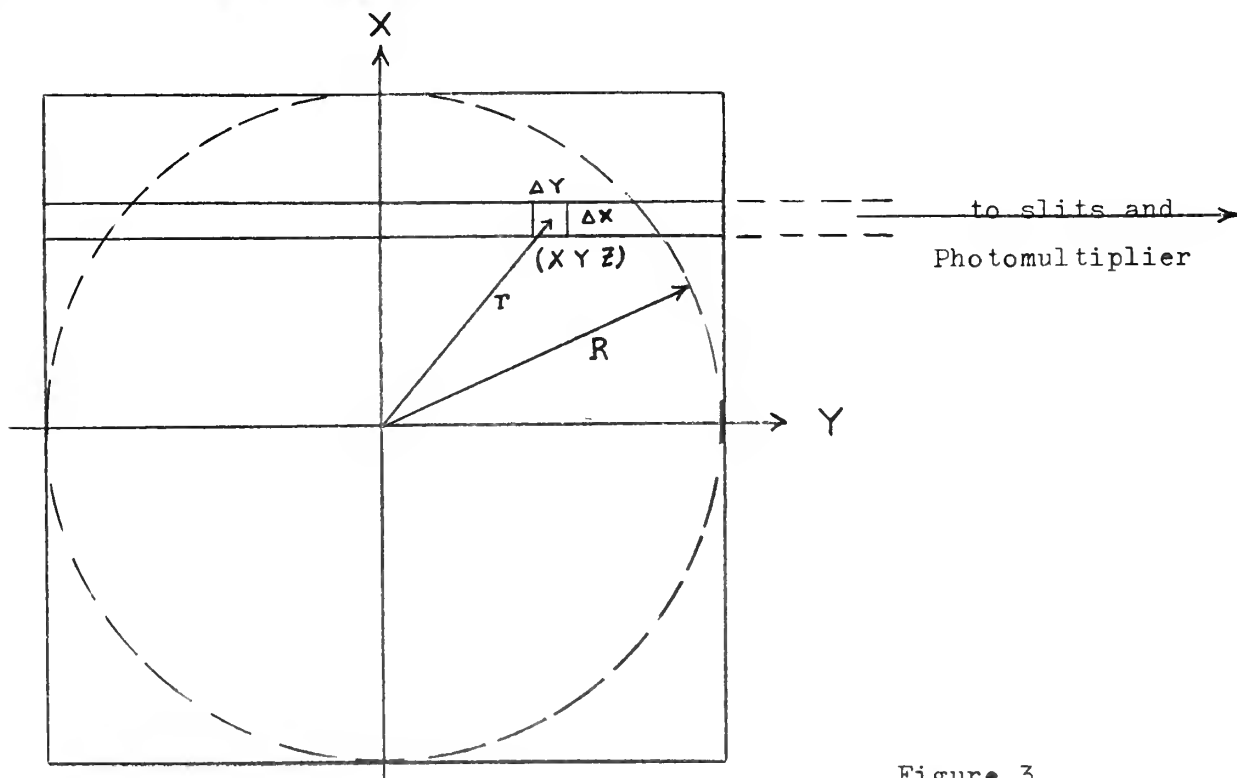


Figure 3

Illustration of the geometrical relationships between the variables

If the horizontal slice is taken at a distance x above the axis and is of height dx and width l , then the total flux falling on the photomultiplier is given by:

$$I(x) l dx = l dx \int_{-Y_0}^{Y_0} f(r) dy \quad \text{Eq. II.2.1}$$

where $f(r) l dy dx$ is that part of the energy which originates in the volume element $l dy dx$ located at a radial distance r from the axis. Since $Y = R^2 - x^2$

$$I(x) = 2 \int_x^R \frac{f(r) r dr}{(r^2 - x^2)^{1/2}} \quad \text{Eq. II.2.2}$$

Equation II.2.2 is one form of Abel's integral equation. This inverts analytically into

$$f(r) = -\frac{1}{\pi} \int_r^R \frac{\frac{dI}{dx} dx}{(x^2 - r^2)^{1/2}} \quad \text{Eq. II.2.2a}$$

In order to smooth the technique, since intensities are measured generally at points and not continuously, Barr reverses the order of differentiation and integration. The final results of Barr's calculations are the formulae:

$$f_k = \frac{1}{\pi \Delta} \sum_{n=k-2}^N \beta_{kn} I_n, \quad k > 2 \quad \text{Eq. II.2.3}$$

$$f_k = \frac{1}{\pi \Delta} \sum_{n=0}^N \beta_{kn} I_n, \quad k \leq 2 \quad \text{Eq. II.2.4}$$

The values of β_{kn} are reported for N up to 20. f_k is the value of radial distribution at station k . Austin and Schrader⁽⁹⁾ have studied the methods of Barr and Bockasten to determine the errors inherent to the numerical analysis employed. The maximum error was determined to be 1.5%, but the average value at each cal-

culated point was 0.1761%.

It should be noted that both Barr's and Bockasten's methods give slightly high values of f_k in the wings of the distributions.⁽⁷⁾

3. Procedure

(Details of the apparatus and the experimental techniques are given in Appendix III.)

Light intensity from an argon discharge was measured by causing the collimated light to fall on the 1P28 photomultiplier. The photomultiplier output was recorded on strip chart paper as the slits vertically scanned the discharge tube.

Several runs were conducted while the tube was not operating to determine the position of the inner walls of the tube as recorded on the strip chart. The error in this determination was estimated to be a maximum of 4%.

The discharge was operated at three pressures and several currents to determine the changes, if any, of the normalized distributions of emitters with changes in these parameters.

Several runs were conducted at each setting of current and pressure. The parameters of the analyzed discharges are given in Figure 4.

Each run selected for analysis was then divided into 20 equal lengths along its time axis, from the center of the intensity curve to the point where the intensity was zero. The ordinates of the curves at these 21 points (station 1 was the axis of the tube) were recorded and then normalized.

These normalized ordinates were also put in a computer program (written primarily by Austin and Schrader⁽⁹⁾) designed to give the

21 values of f_k (the value of the normalized radial distribution at station k) in formulae II.2.3 and II.2.4. These normalized outputs were plotted to give the radial distribution of emitters out to zero intensity.

Run	Pressure (Torr)	Current (Amperes)	Tube Voltage (Volts)	Striations
CR	26.47	0.315	145	Starting
ER	26.47	0.600	119	No
GR	26.47	1.100	103	No
HR	26.47	1.180	99	No
JR	18.48	0.600	105	No
LR	18.48	1.100	91.3	No
MR	18.48	1.210	89	No
OR	18.48	0.451	112	Starting
QR	18.48	0.300	128	Yes
SR	8.88	0.600	81	Yes
VR	8.88	0.300	92.5	Yes
YR	8.88	1.100	73	No

Figure 4

Parameters of Analyzed Discharges

Each of the runs selected for analysis were again divided into 20 equal sections along its time axis; but this time the 20 parts were each one-twentieth of the run of the inner radius of the tube. The ordinates were again measured, normalized, and plotted. (See Appendix I)

These normalized ordinate distributions measured out to the radius of the tube were also put in the above mentioned computer

program to determine the f_k s of Equations II.2.3 and II.2.4. These normalized values were also plotted to give the radial distribution out to the inner surface of the tube. (See Appendix II)

The curves which were plotted for normalized intensity and f_k to zero intensity are not included in this report as they proved to give no information not given by the curves in Appendices I and II.

4. Analysis of Data

The above procedure was made possible by the discovery that the great asymmetry in intensity patterns about the axis of the tube, in the original runs, was due to polarized light. This polarized light phenomena was demonstrated by recording intensity patterns with the regular slits covered with a polaroid. Polarization is not expected in the positive column.⁽¹⁾ Investigation showed that this polarization effect was due to the fact that some light detected was reflected from the walls of the square section.

This asymmetry was greatly reduced by placing adjustment screws in the base plate of the drive motor stand (see Figure 9), and adjusting them until the line of sight through the slits was perpendicular to the the square glass side. This procedure removed all asymmetry except that near the top edge of the tube, where the intensity was somewhat greater than that near the bottom edge of the tube. This asymmetry is believed to be due to slight irregularities in the glass. For these reasons all intensity runs were analyzed only on the bottom half of the tube to give more comparable results.

In analyzing the normalized radial distribution curves in Appendix II several considerations are proper in assigning weighting

factors to the various runs.

Runs RR, SR, VR, and YR had the shortest amplitude on the strip chart of any runs analyzed. Any errors in the measurement of the ordinates of these curves at the 21 stations are more amplified in normalization and the curves therefore are less reliable than the others.

The validity of the determination of f_k out to the inner surface of the tube also deserves inspection. The R in formula II.2.2 is the radius beyond which $f(r)$ is negligible. Several runs, CR, ER, and QR showed f_k falling to zero before station 21. f_{20} was zero in runs CR and ER and f_{19} was zero in run QR. The accuracy of these runs is therefore suspected to be somewhat less than the others.

A consideration applicable to all runs is that the section of the tube which was observed was not a cylinder, but a square. Since the discharge tends to fill the square tube, the intensity and radial distributions will be greater near the tube wall than would these distributions in a cylindrical tube. Furthermore, this effect will influence the distributions of the high current and/or low pressure runs more than the low current and/or high pressure runs. However, this effect is produced only in the very high f_k s (those near the wall) as Equation II.2.3 illustrates. In addition, it may be seen by observing the graphs that the large variations in normalized distributions do not occur near the tube wall.

A final consideration is the width of the slits used in collimating the light. The slits were .750 mm wide. The interior square tube width was 20 mm. There were therefore only 13.3 possible

stations if these slits could be placed accurately along the tube for static measurements.

The width of the slit did not permit good definition of sharp changes in intensity. This was demonstrated by the fact that when an opaque rubber section with a sharp edge was placed along the glass, the intensity plot showed no step function but was a linear function of distance from the edge. Figure 5 shows that the observed beam of light was actually even greater than 750 microns.

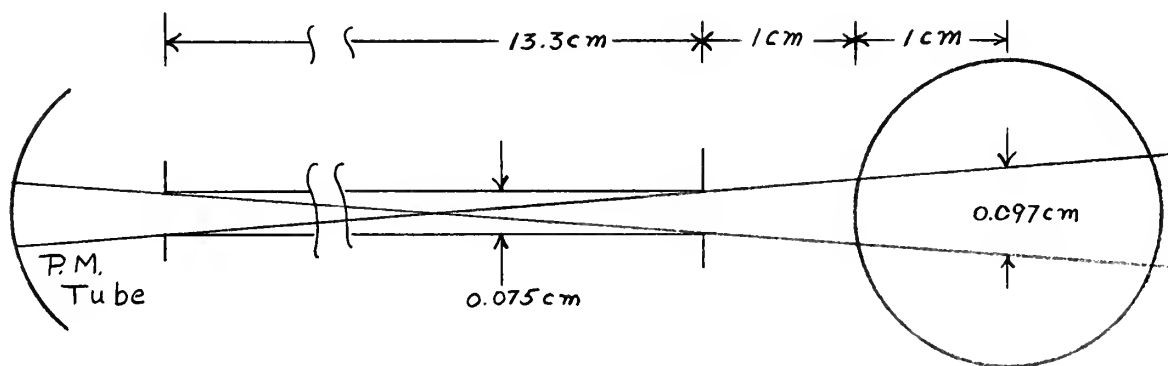


Figure 5

Cone of light falling on the photomultiplier surface.

5. Results

Analysis of the curves in Appendix II shows that there was a greater portion of the emitters further out from the axis as the pressures decreased (constant current) and as the current increased (constant pressure). No analytical expression has been given for the general set of curves, but it is clear that the distribution of emitters approached the zero order Bessel function⁽⁸⁾ as pressures decreased and currents increased. The zero order Bessel function is plotted in Appendix II in order to show this relation. It is

shown in section II that this is the distribution predicted by von Engel for electrons and ions.

As Figure 2 shows, there is a radial variation in the temperature of the electrons. Therefore there is no one-to-one correspondence between electron density and excited atom density since the cross sections for excitation are a function of electron energy. However, the electron temperature is nearly constant at low pressures, and it is at these pressures that the distribution of emitters approaches the zero order Bessel function. This would indicate that the electron distribution is then also near a zero order Bessel function.

There appears to be no significant variation of radial emitter distributions connected with the striations in the tube. Throughout this series of runs and others (see Appendix II, Runs OR and QR), large variations in operating conditions did not change the regular variation of the distribution of emitters.

6. Recommendations for Further Work

The apparatus used in this work did not permit very high resolution of radial distribution. It is therefore recommended that a collimator with greater spatial resolution be used in further efforts to define radial distributions of emitters. It is also recommended that their distributions be measured at various bands of wavelength. It may be profitable to construct a tube with an inner cylindrical tube having an outside diameter equal to the 20mm inside width of the square section. Additionally, instead of a complete disk-like gap as in tube 2, it may furthermore decrease error by having only a semi-circular disk removed from the inner tube.

7. Acknowledgements

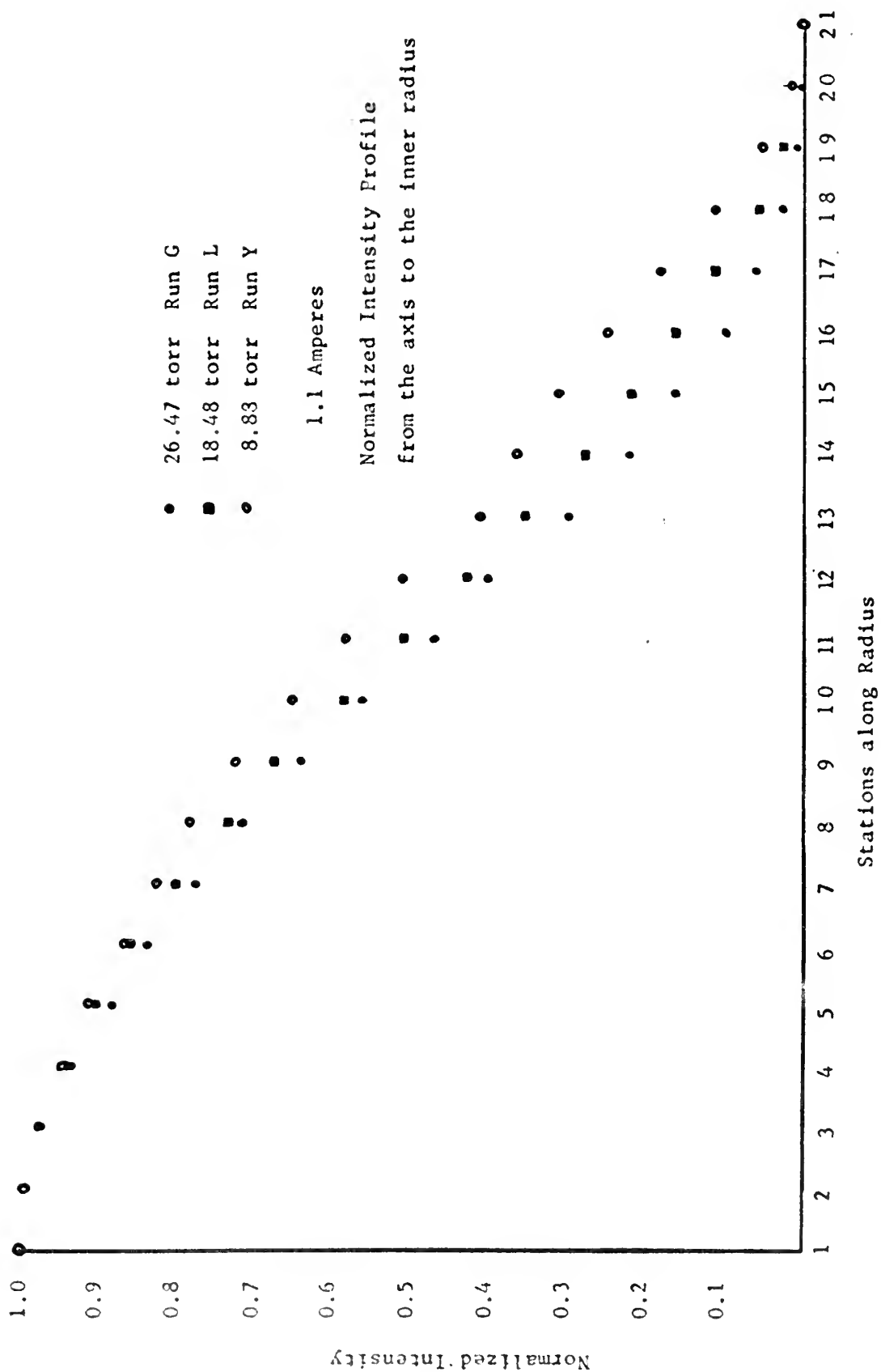
The writer wishes to express his appreciation to Professor R. L. Kelly for his guidance and assistance throughout this work, to Professor S. H. Kalmbach for his advice and help, particularly in solving problems connected with the optical system, and to Professor A. W. Cooper for his counsel. I also gratefully acknowledge the technical assistance of Messieurs M. K. Andrews, R. C. Smith, and J. Calder.

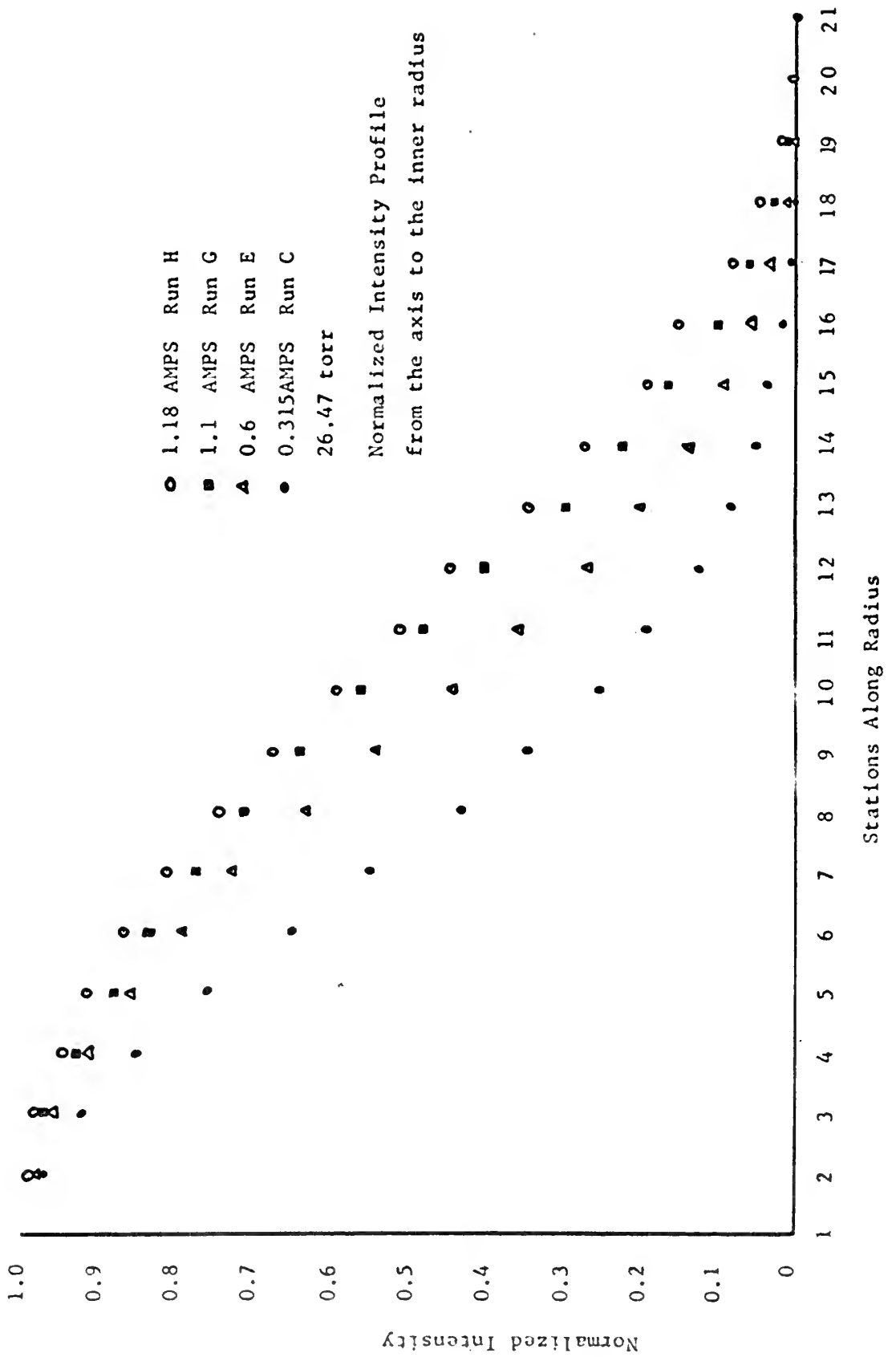
BIBLIOGRAPHY

1. A. von Engel, Ionized Gasses, (Oxford at the Clarendon Press, 1955).
2. Sanborn C. Brown, Basic Data of Plasma Physics, (M.I.T. Press and John Wiley and Sons, Inc., New York 1959), p.311.
3. A Course Given by S. Chandrasekhar, Plasma Physics, (Notes compiled by S. K. Trehan, The University of Chicago Press 1960), p.139.
4. D. J. Rose and M. Clark, Jr., Plasmas and Controlled Fusion, (M.I.T. Press and John Wiley and Sons, Inc., New York 1961), p. 185.
5. K. Bockasten, J. Opt. Soc. Am. 51, 943 (1961).
6. F. H. M. Kinley and R. J. O'Malia, A Spectroscopic Investigation of an Argon Glow Discharge, (M. S. Thesis, U. S. Naval Postgraduate School, 1962).
7. W. L. Barr, J. Opt. Soc. Am. 52, 885 (1962).
8. J. W. McClain, F. C. Schoenig, Jr., and N. J. Palladino, Table of Bessel Functions to Argument 85, (Pennsylvania State University Press, University Park, 1962), p.8.
9. R. C. Austin and H. C. Schrader, Jr., A Spectroscopic Investigation of an Argon Glow Discharge, (M. S. Thesis, U. S. Naval Postgraduate School, 1962).
10. Sanborn C. Brown, (Chairman), American Journal of Physics 31, 638 (1963).

APPENDIX I

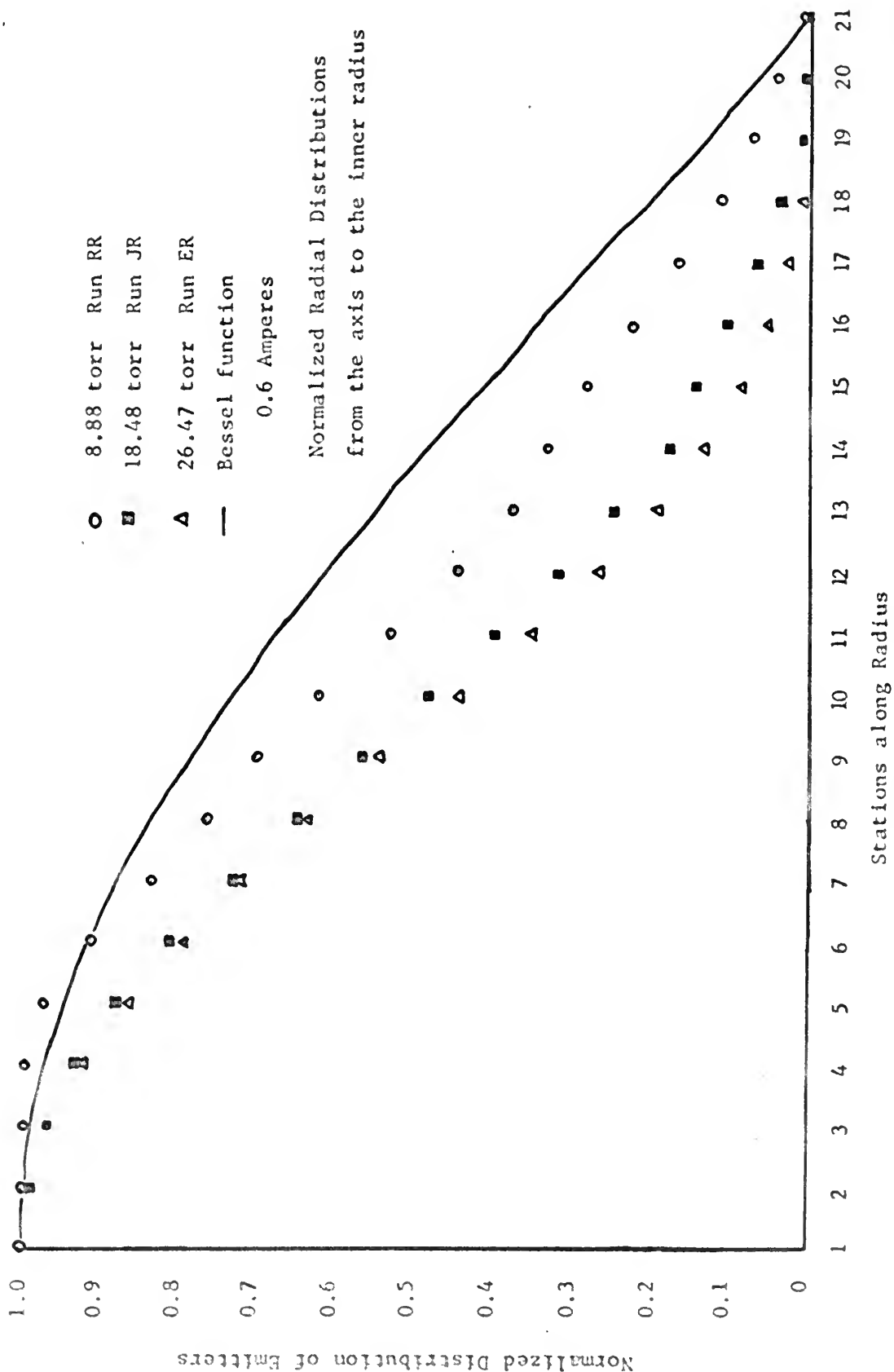
Normalized Intensity of Light
from the Axis to the Inner Radius of the Tube

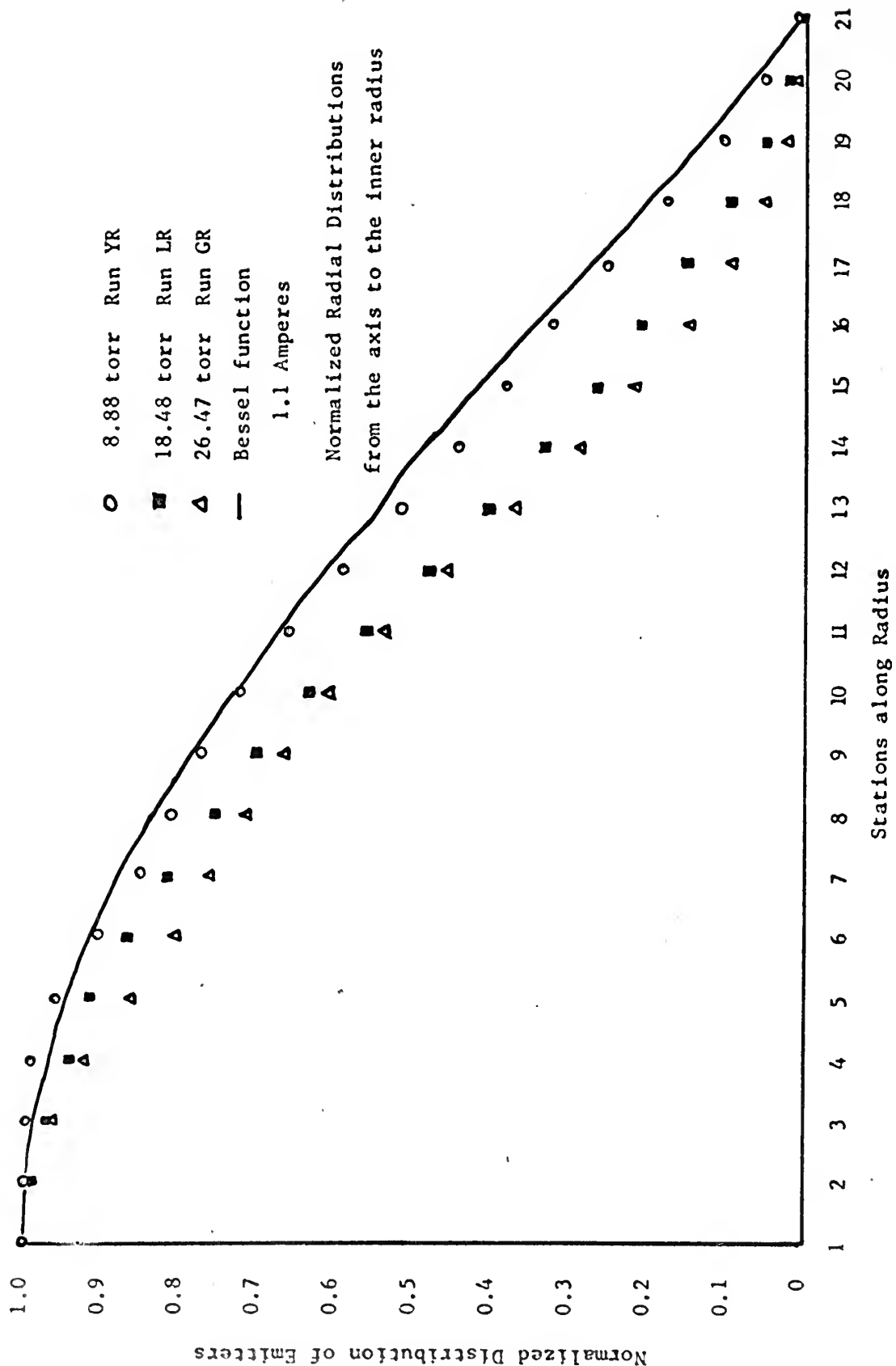


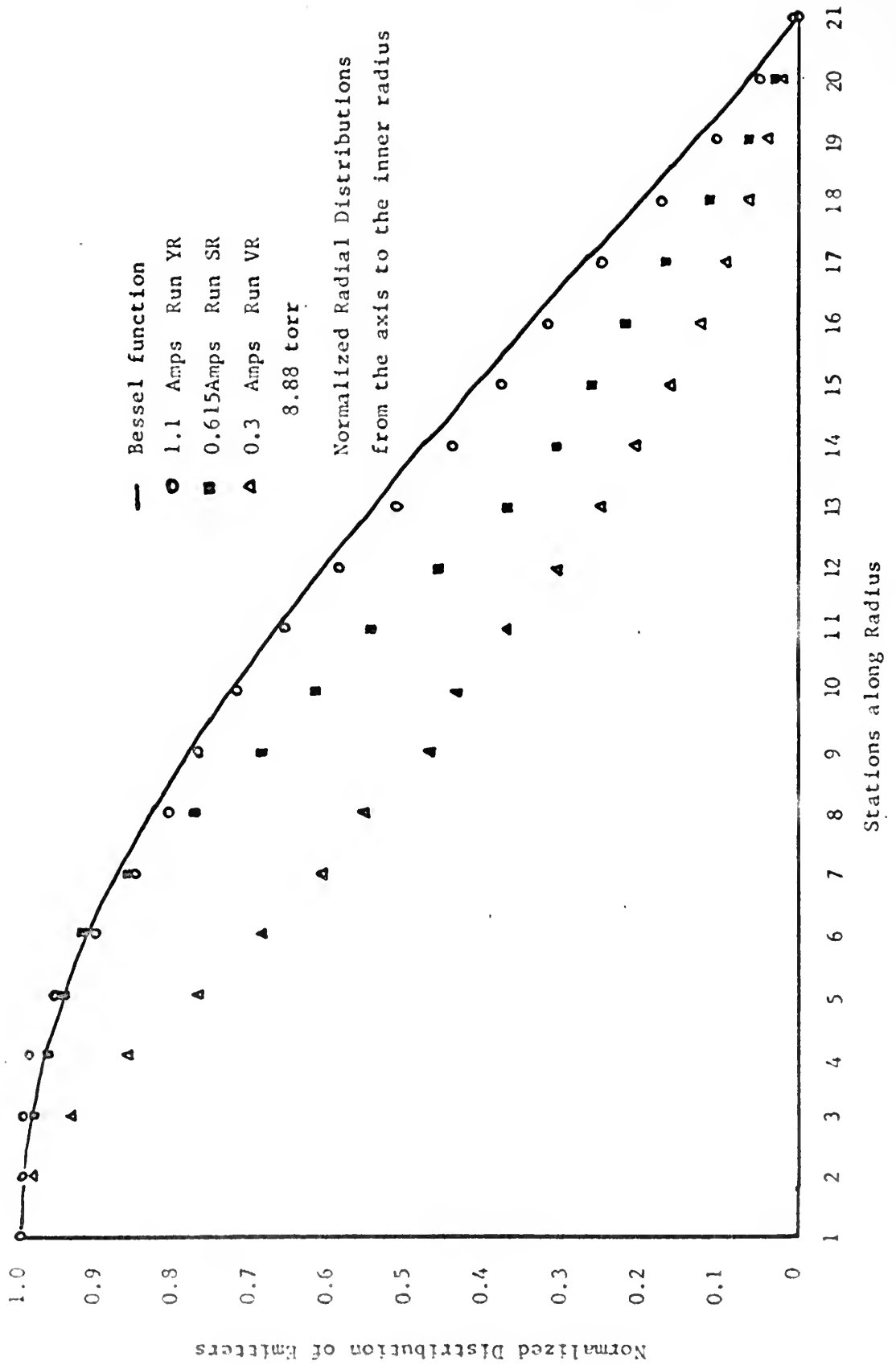


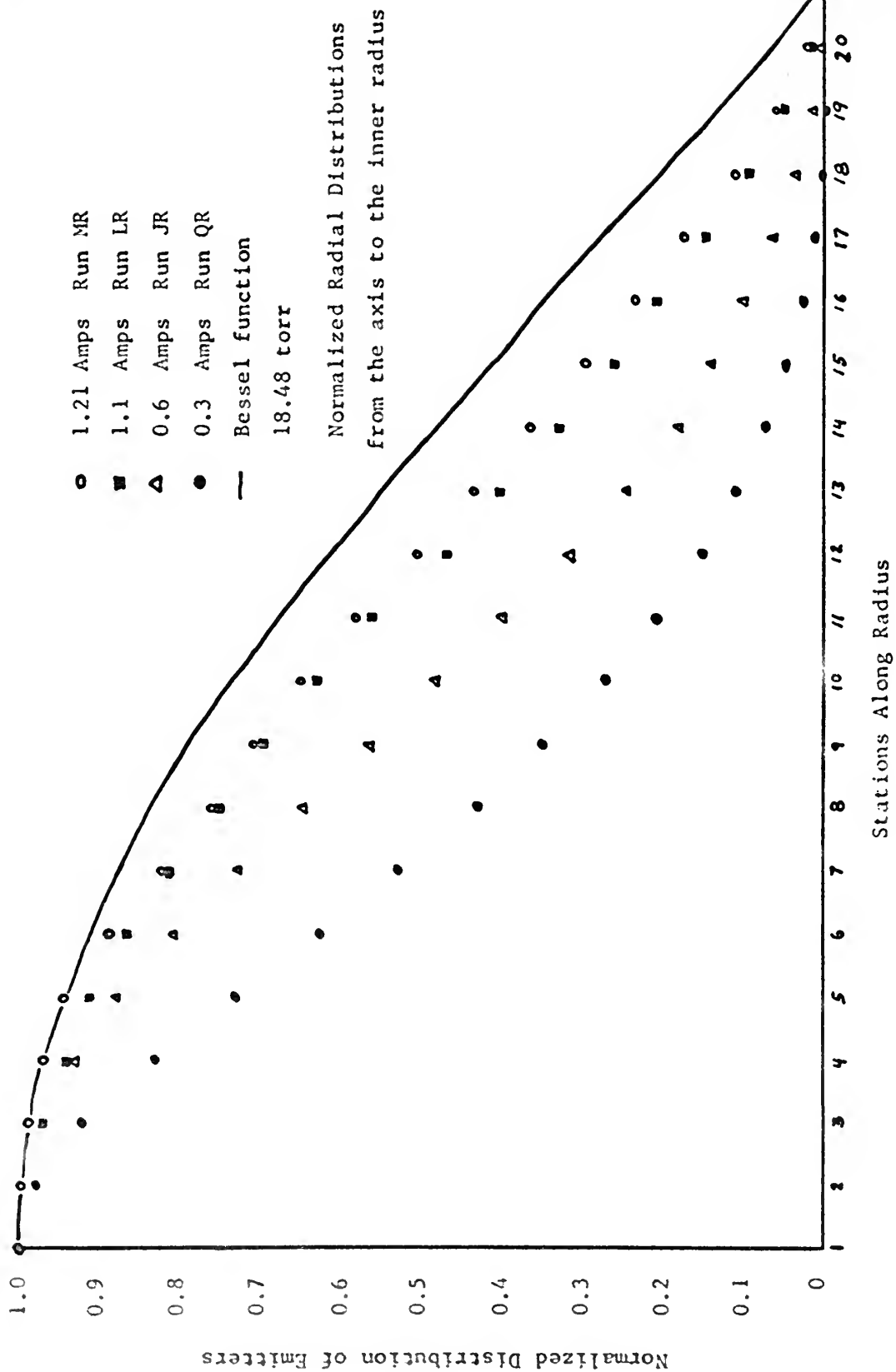
APPENDIX II

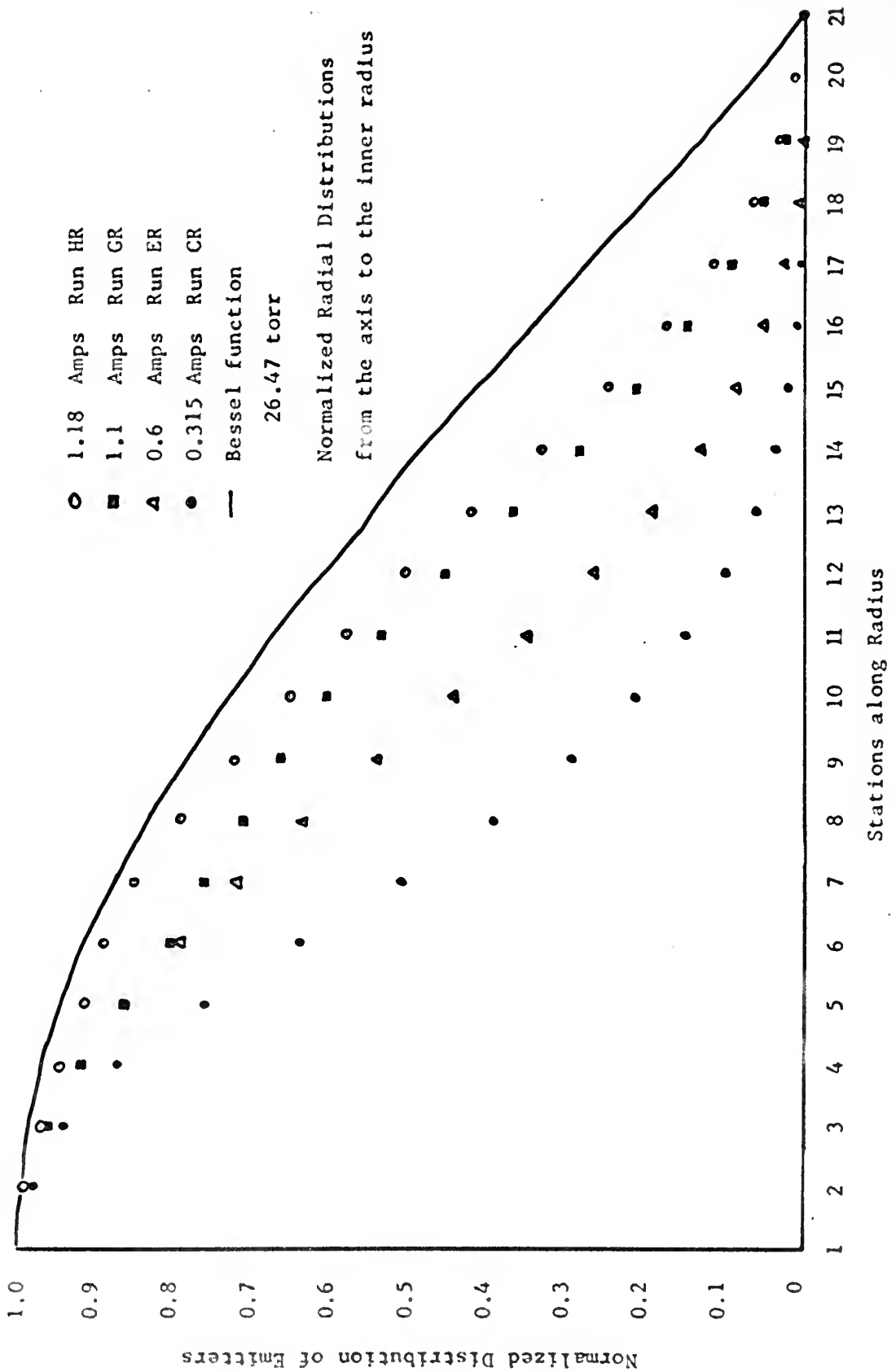
Normalized Radial Distributions
from the Axis to the Inner Radius of the Tube

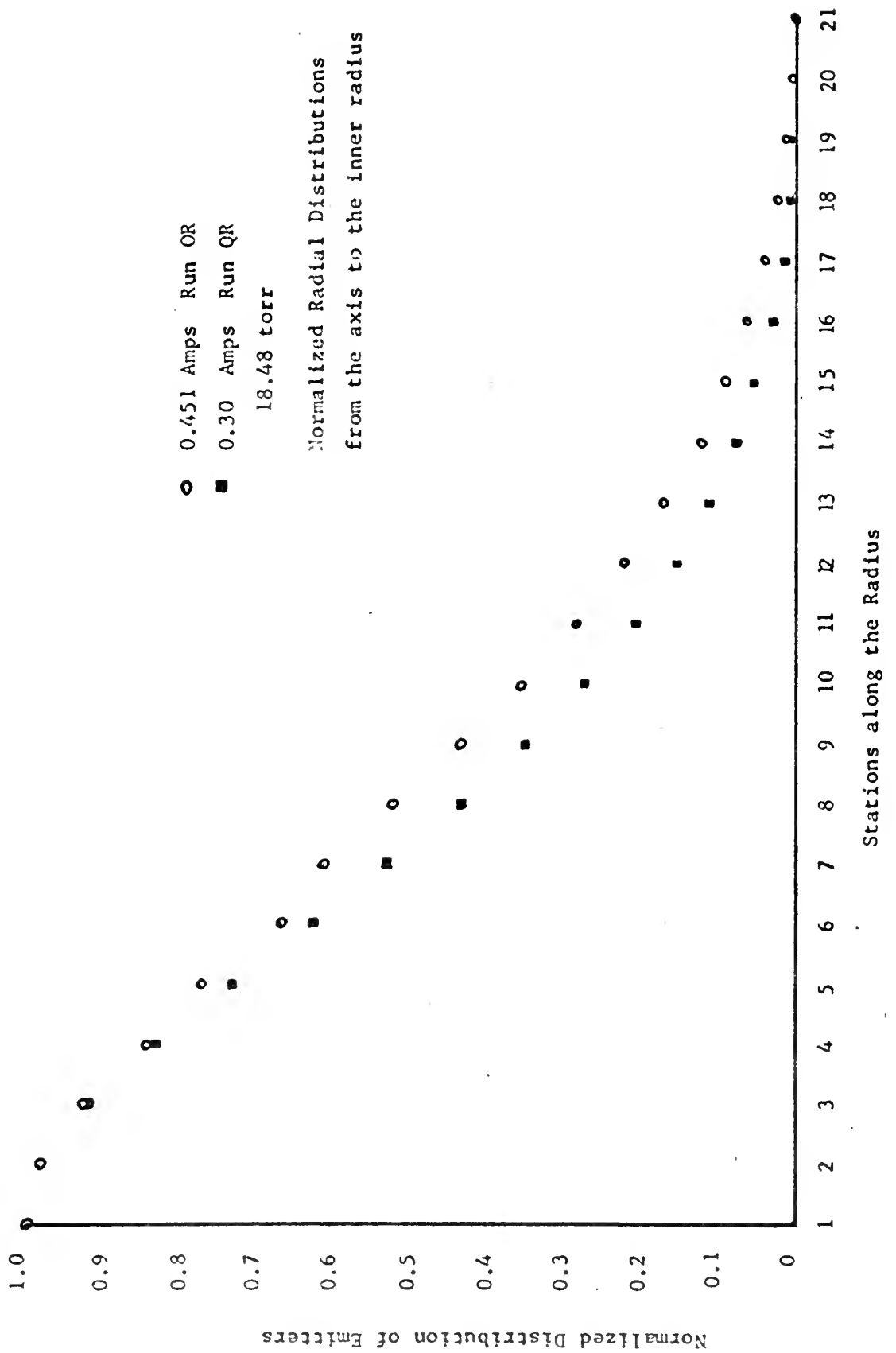












APPENDIX III

APPARATUS AND EXPERIMENTAL TECHNIQUES

1. Vacuum System and Gas Filling Systems

The discharge tubes were horizontally mounted on an all-glass vacuum system designed to reach pressures in the order of 10^{-6} to 10^{-7} mm. A schematic diagram of the vacuum and gas filling systems is shown in Figure 7. These pressures were obtained with the following equipment:

- a. A Welch Duo-Seal pump for a forepump.
- b. A three-stage air-cooled Consolidated Vacuum Corp. type GF-26 diffusion pump using Octoil-S vacuum pump fluid.

- c. A liquid air trap at the vacuum side of the diffusion pump.

Overall and close-up views of the vacuum system and associated equipment are given in Figures 8, 10, and 11.

De-gassing of the tube walls and electrodes was essential to achieve and maintain a high degree of purity of the discharge gas. De-gassing was accomplished, under high vacuum, by the repeated techniques of:

- a. Heating the entire tube for several hours with electrical heating tapes.

- b. Heating the nickel electrodes until red with an induction heating generator.

- c. Heating the tungsten filaments with 8 ampere currents. (7.5 amperes were used when the discharge was operating.)

- d. Filling the tube with Argon and operating it for short periods. This was repeated until a pure discharge was obtained.

A one-liter pyrex glass flask of Linde high-purity gas at

at about one atmosphere pressure was sealed into the system, and filling was accomplished by means of a pair of stopcocks on either side of an small feeding bulb.

The gas pressures in the tubes were measured with a 100 cm. Octoil-S manometer (1cm. oil = 0.672 mm. Hg.).

2. Power Supply and Instrumentation

A schematic diagram of the power supply circuit is shown in Figure 6.

A continuous direct current discharge was maintained and appropriate measurements made by use of the following equipment:

a. The discharge tube voltage was supplied by a Kepco Labs. Model 770B power supply which produced output voltages continuously up to 600V D. C. Tube currents were measured by an ammeter (0-3 amperes) built into this power supply.

b. A Pupps discharge was maintained at the anode between the two electrodes to improve stability. Power for this was supplied by a Kepco Labs. Model 500R-B Power Supply (0-600 volts, 0-300 milliamperes).

c. The cathode was heated by a Kepco Labs. Model KM 236-15A Power Supply (0-50 volts, 0-15 amperes).

d. Pressures were determined by use of a thermocouple gauge tube at the forepump and by a Consolidated Vacuum Corp. type GIC-110 VG1A ion gauge on the discharge tube side of the cold trap.

e. Relative light intensity was determined by collimating the light from the discharge with two 750-micron slits, and by having this light fall on an RCA 1P28 photomultiplier tube. The 1P28 was covered with mu metal to help reduce noise. The output

from this tube was the input to a Baird Atomics 100 millivolt recorder.

f. A second photomultiplier, an RCA 1P22, was used to determine if the discharge had moving striations in it at the time the measurements were being made. The output from this 1P22 was put into a type 545A oscilloscope.

g. 1P28 power was supplied by a Baird Atomic photomultiplier Supply Model 312A. 1P22 power was supplied by a locally constructed power supply unit. (0-2 kilovolts negative output)

h. Tube voltages were measured with a Westinghouse type PX-5 D. C. Voltmeter (200 ohms/volt).

i. The photomultiplier and slits were mounted on a small platform with the slits 13.3 cm. apart. This platform was driven vertically by a Bodine synchronous motor type NC1-12R. All gears and threads associated with the drive were of high precision to ensure constancy of vertical movement. The motor was shock-mounted to an aluminum plate which served as a base for the vertically driven platform. This plate had screw mountings which permitted the spectograph slits to be accurately aligned both longitudinally along the tube and perpendicular to flat glass faces where the tube was studied. (This perpendicularity appears to be very important and is discussed in the procedure section.) A close-up view of the slits, photomultiplier, and drive is given by Figure 9.

3. Glass Discharge Tubes

Two specially designed pyrex glass tubes were constructed to remove any effect of variation in the glass absorption and reflec-

tion effects. The first tube studied (called tube 1) consisted of a circular glass tube of inside diameter 21.7 mm., outside diameter 24.9 mm. A 31 mm. long section of precision square cross section (20 mm. inside width) tubing was fused into the discharge tube near the middle. The circular tubing ended where fused to the square section. (See Figure 12)

The second tube (called tube 2) differed from tube 1 in two ways. The inside diameter of tube 2 was 13.7 mm. and outside diameter 16 mm. A 5.7 cm. section of the precision square cross section (20 mm. inside width) tubing was also fused to this circular tube near its center. However, the circular tubing did not end at the point of fusing, but continued into the 20 mm. square section. The circular tubes were separated by about 5 mm. The tube ends were not exactly parallel. (See Figure 12)

The electrodes on each end of the tubes were identical. The electrodes were constructed so that they could be used as either cathode or anode in order to give a prolonged lifetime to the tubes. Each end therefore had a cylindrical nickel electrode and within this was a tungsten coiled wire electrode.

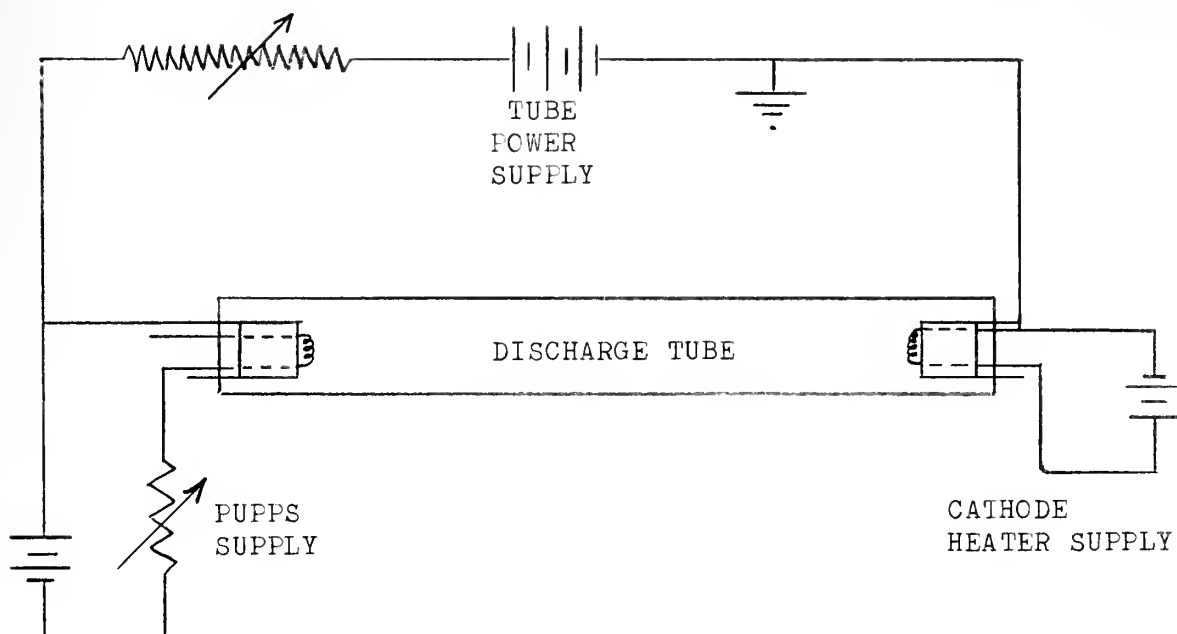


Figure 6

Schematic Diagram of Power Supply

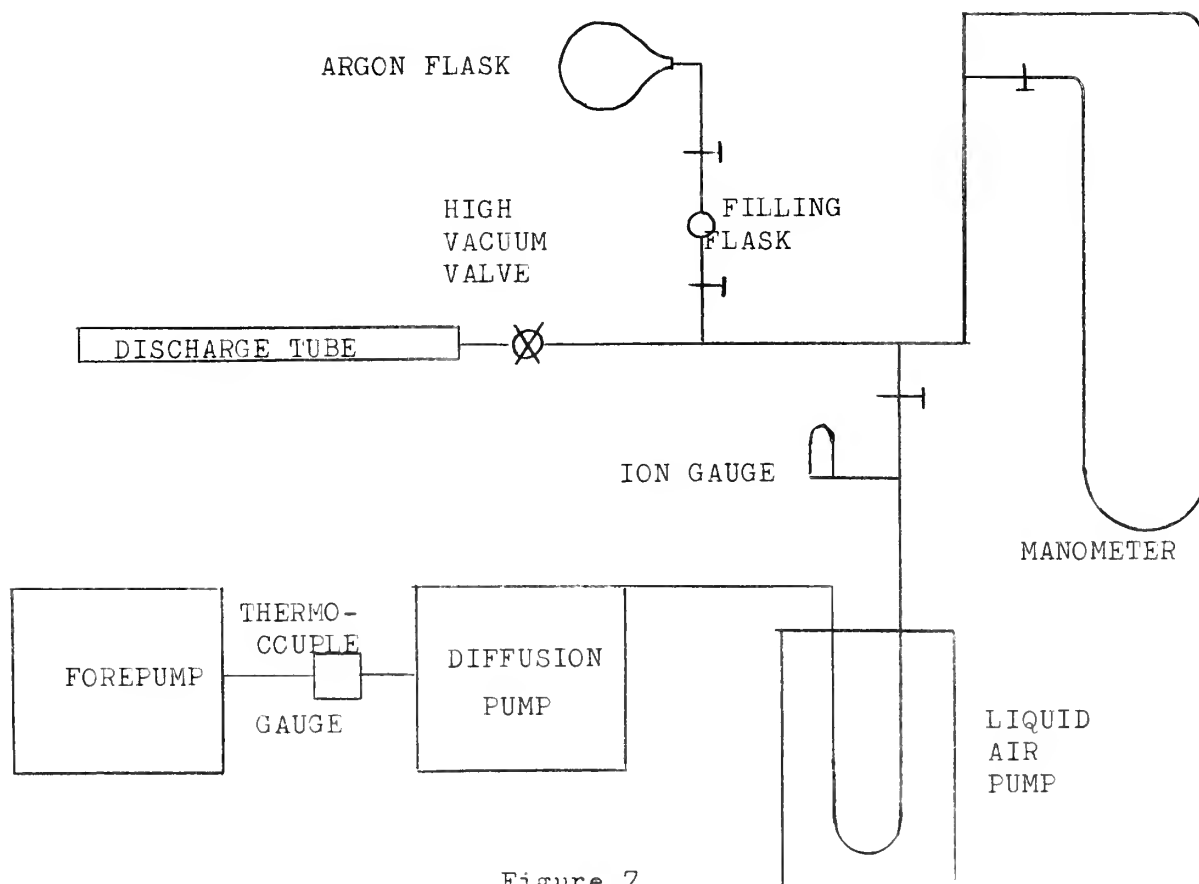


Figure 7

Schematic Diagram of Vacuum System

Key to Apparatus in Figures 8, 9, 10, 11, 12

1. Discharge Tube #1
2. Discharge Tube #2
3. 1P22 Photomultiplier with Cover
4. Stand and Synchronous Motor Drive for Slits and 1P28
5. Power Supply for 1P28
6. Power Supply for Discharge Tube
7. Power Supply for Pupps Discharge (below this and not visible is the 1P22 Power Supply and the Cathode Heater Power Supply)
8. Meter for Ionization Gauge
9. Tesla Coil
10. Oscilloscope
11. Ionization Gauge
12. Thermocouple Gauge
13. Forepump
14. Diffusion Pump
15. Strip Chart Recorder
16. Induction Heater
17. Heating Tapes
18. Heat Gun
19. Liquid Air Trap
20. Dehumidifier
21. Meter for Thermocouple



Figure 1 (Overall view of the equipment)

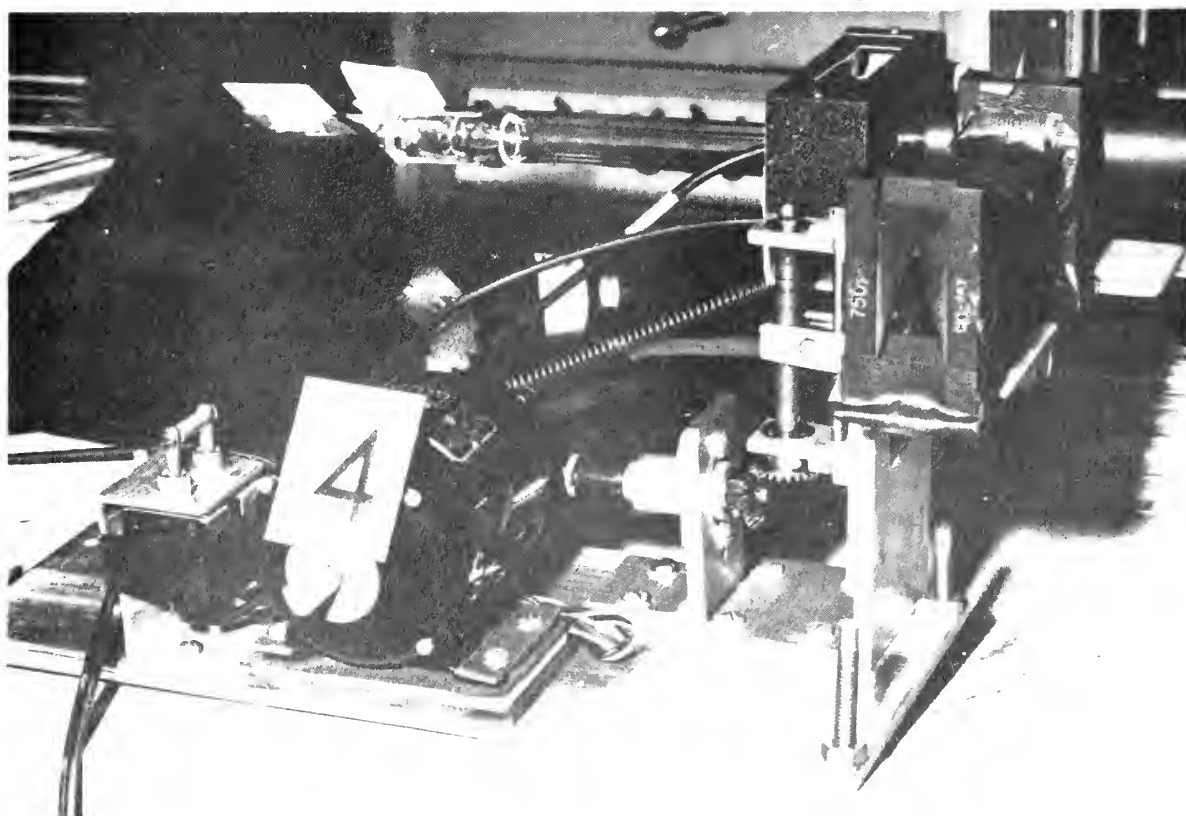


Figure 2 (Close view of the pump device)

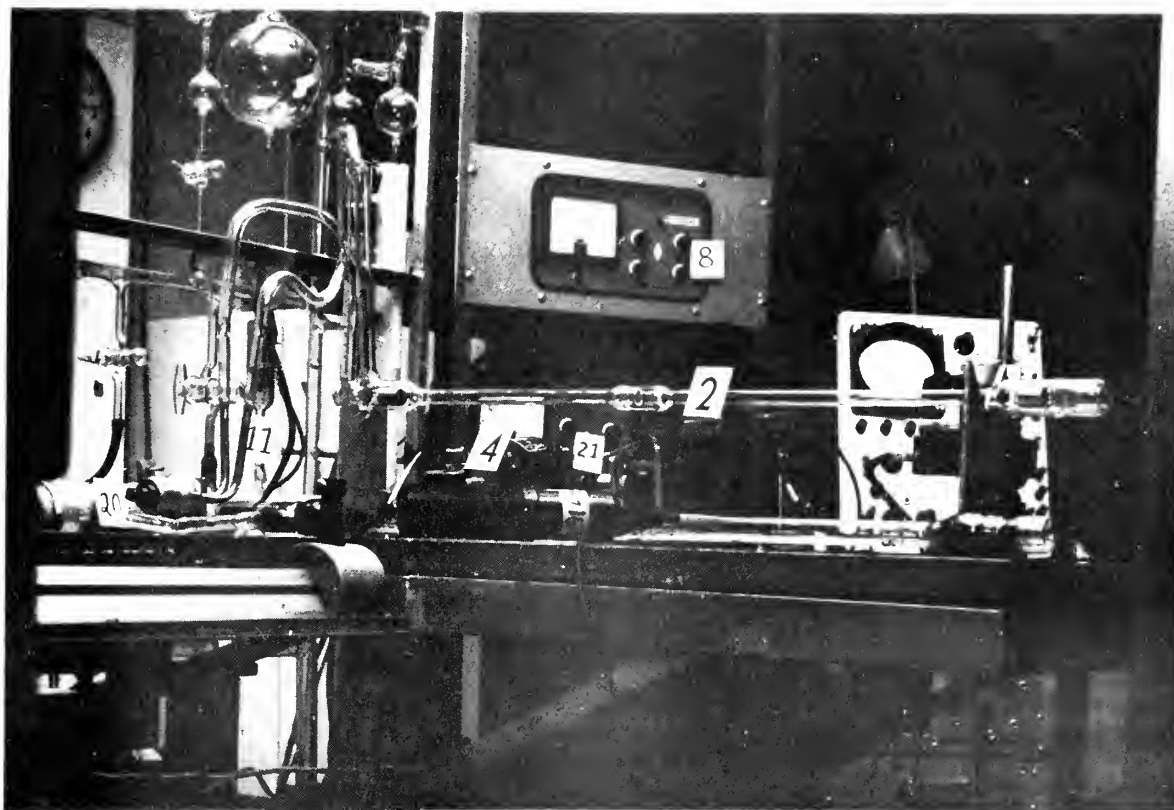


Figure 10 View of the Working Platform

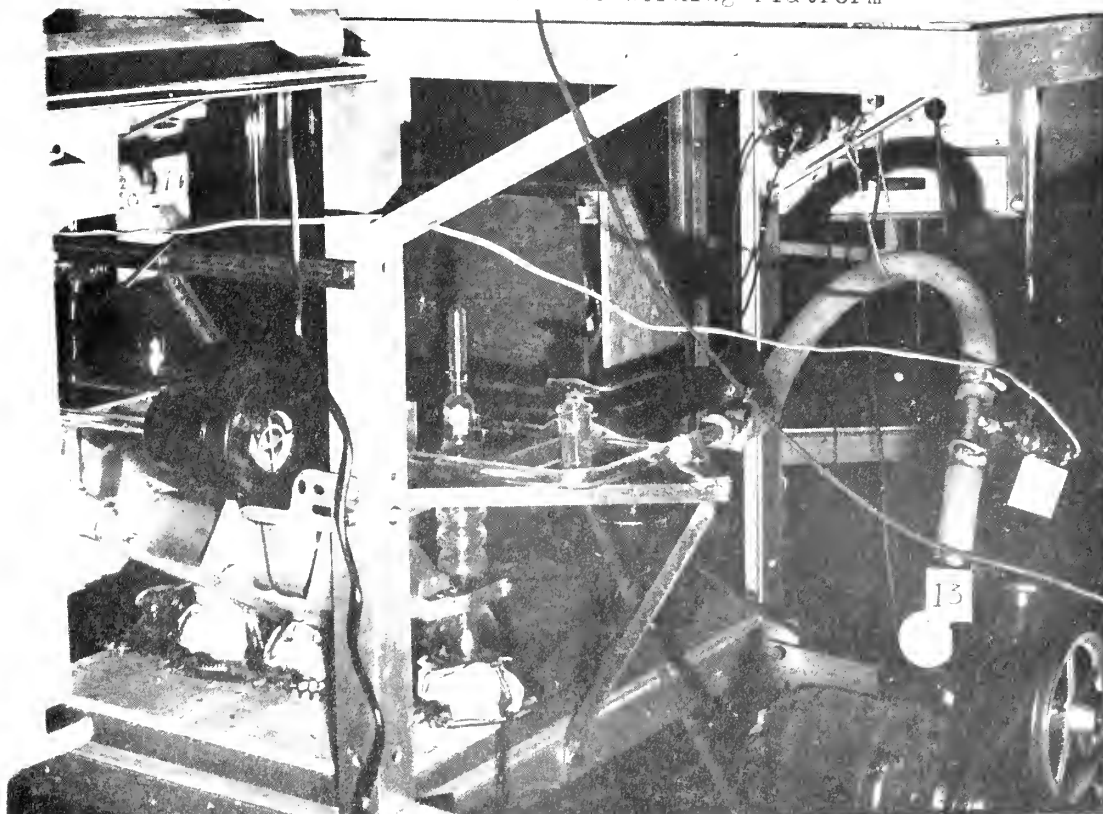


Figure 11 View of Diffusion Pump and Forepump

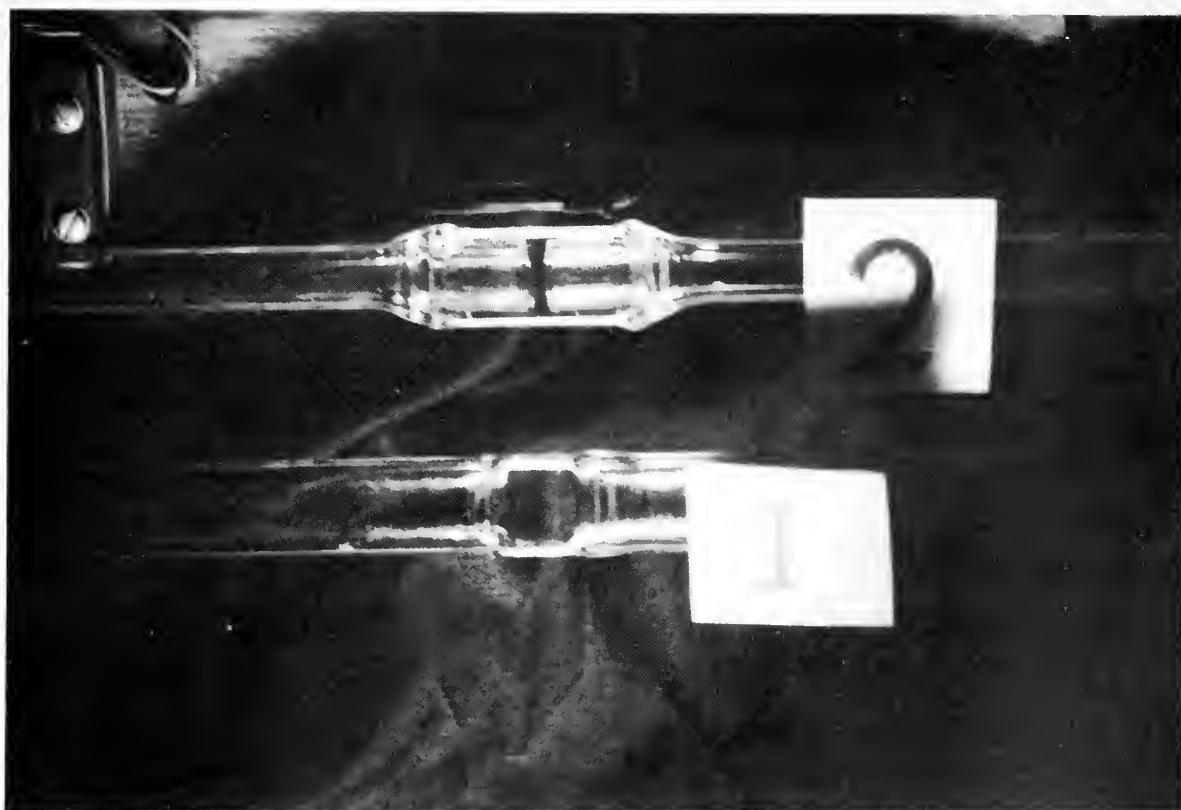


Figure 10 Close view of Tubes 1 and 2

